ACS OMEGA

Open Access

http://pubs.acs.org/journal/acsodf

Article

One-Step Physical and Chemical Dual-Reinforcement with Hydrophobic Drug Delivery in Gelatin Hydrogels for Antibacterial Wound Healing

Di An, Zhengkai Wang, Yishuo Ning, Yuxing Yue, Han Xuan, Yongjin Hu, Mingdi Yang, Haiou Zhou, Qianqian Liu, Xianbiao Wang, Ping Wang, Zhiyuan Zhu,* Jingyi Rao,* and Jingyan Zhang*

Cite This: *ACS Omega* 2024, 9, 34413−34427

Read Online

ACCESS | Metrics & More | Article Recommendations

ABSTRACT: Gelatin-based bioadhesives, especially methacrylated gelatin (GelMA), have emerged as superior alternatives to sutureless wound closure. Nowadays, their mechanical improvement and therapeutic delivery, particularly for hydrophobic antibiotics, have received ever-increasing interest. Herein, a reinforced gelatin-based hydrogel with a hydrophobic drug delivery property for skin wound treatment was reported. First, photosensitive monomers of *N*′-(2-nitrobenzyl)-*N*-acryloyl glycinamide (*NB*NAGA) were grafted onto GelMA *via* Michael addition, namely, GelMA-*NB*NAGA. Second, gelation of the GelMA-*NB*NAGA solution was accomplished in a few seconds under one step of ultraviolet (UV) light irradiation. Multiple effects were realized simultaneously, including chemical cross-linking initiated by lithium phenyl-2,4,6-trimethylbenzoylphosphinate (LAP), physical cross-linking of uncaged dual hydrogen bonding, and hydrophobic drug release along with *o-NB* group disintegration. The mechanical properties of the dual-reinforcement hydrogels were verified to be superior to those only with a chemical or physical single-cross-linked network. The hydrophobic anticancer doxorubicin (DOX) and antibiotic rifampicin (Rif) were successfully charged into the hydrogels, separately. The *in vitro* antimicrobial tests confirmed the antibacterial activity of the hydrogels against Gram-negative (*Escherichia coli*) and Gram-positive (*Staphylococcus aureus*) bacteria. The *in vivo* wound-healing assessment in mice further assured their drug release and efficacy. Therefore, this *NB*NAGA-modified GelMA hydrogel has potential as a material in skin wound dressing with a hydrophobic antibiotic on-demand delivery.

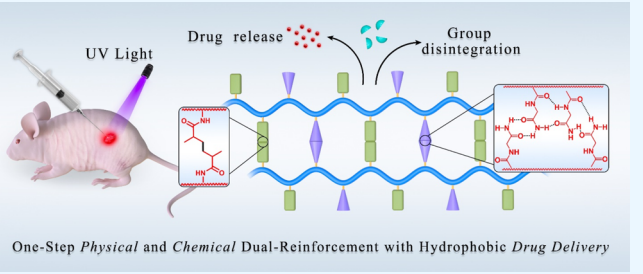

1. INTRODUCTION

As the largest organ of the human body, the skin is extremely important for body protection, sweating excretion, temperature regulation, and external stimuli feeling, which is exactly the reason for being one of the most vulnerable tissues.[1−3] Wound dressings bind and cover damage, providing a temporary barrier from microbial invasion, cross-infection, and so on. Moreover, they serve as an induction template to guide the reorganization of skin cells and subsequent infiltration and integration of host tissues, showing a significant effect on wound healing.[4−9]

Hydrogels, the most competitive materials for wound dressings, possess diverse advantages, such as porous network, soft nature, shape maintenance, superior hydrophilicity, and favorable biocompatibility. Among them, structures like an extracellular matrix (ECM) facilitate the broad application of hydrogels in wound healing.[10−15] In peculiar, hydrogels from naturally derived proteins are extensively used to fabricate tissue adhesives for their excellent coordination with the human body.[16−20] As a representative material of this glass of adhesives, gelatin is the irreversibly hydrolyzed form of collagen with a broad range of molecular weights depending on the denaturation method. In general, gelatin is soluble in warm water above 40 °C, but on cooling, thermoreversible transparent gels are normally formed accompanied by a partial regain of the collagen triple-helix structure. Its biodegradability and inflammation properties without antigenicity lead to its wide use in pharmaceutical and medical applications.[21]

An ideal skin wound dressing needs to meet several requirements, including low toxicity or inflammation, sufficient mechanical strength, and appropriate biochemical function for cell proliferation and differentiation.[22] Since gelatin gels have a relatively low melting point, they are not stable at body temperature. Therefore, a variety of hardening procedures were

Received: February 28, 2024
Revised: July 17, 2024
Accepted: July 18, 2024
Published: July 29, 2024

Scheme 1. Schematic Illustrations of the Preparation of Drug-Loaded Hydrogels and the Process of Wound Healing[a]

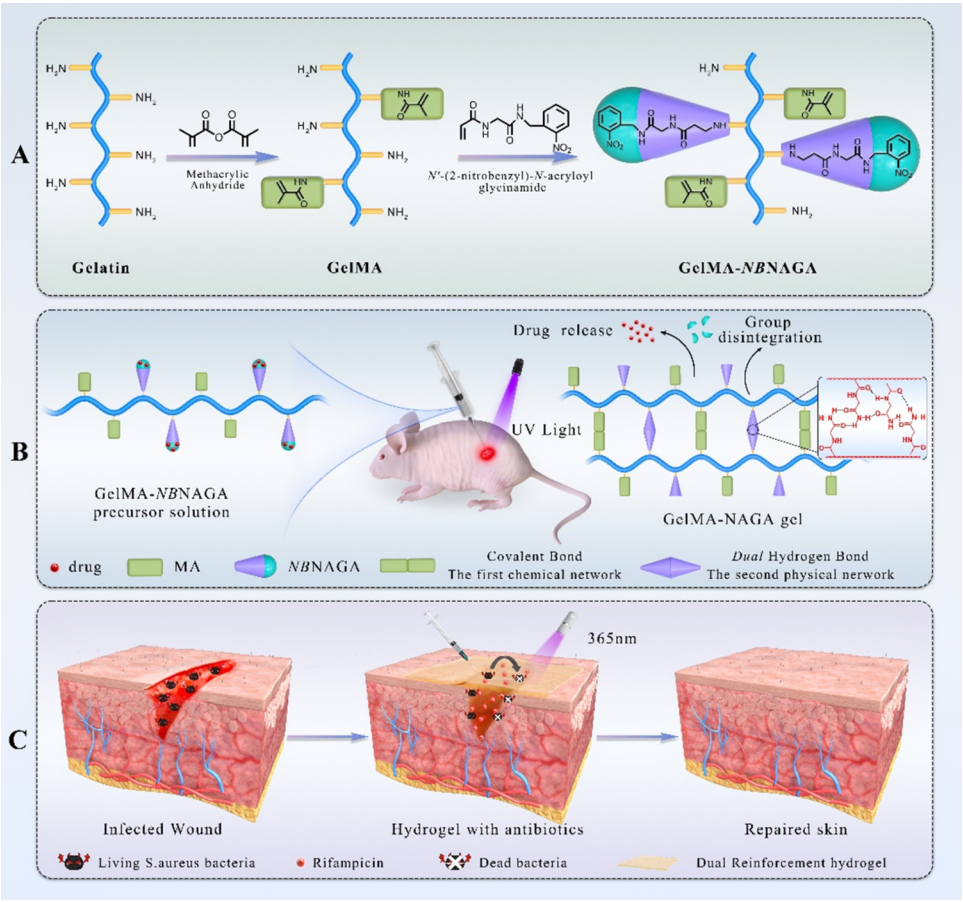

[a](A) Schematic for the synthesis of GelMA and GelMA-*NB*NAGA. (B) Gelation of the GelMA-*NB*NAGA solution containing drugs *in situ* by chemical and physical dual-cross-linking network under irradiation of UV light. (C) Process of wound healing with antibiotic hydrogel treatment.

described in the literature by establishing further cross-links between the protein chains.[23,24] As the most well-known instance, the chemically reinforced reaction originated from side groups on gelatin with the bifunctional glutaraldehyde.[25] Afterward, a polymeric cross-linker, dextran dialdehyde, was developed for chemical aging for gelatin hydrogels.[26] Nowadays, a more attractive concept of methacrylamide-modified gelatin (GelMA) was raised by Van Den Bulcke et al.[27] since chemically stable materials are conveniently formed by ultraviolet (UV) irradiation in the presence of a water-soluble photoinitiator as a "smart" hydrogel. Its unique advantages, including low cost and easy production, contribute to its extensive application as a promising bioadhesive for skin repair.[28−39] Current research interests focus on incorporating diverse functions into the GelMA network for significant clinical utility. Recently, Zhu's research group introduced UV light-sensitive group-modified hyaluronic acid (HA-NB) into the GelMA hydrogel. The phototriggered imine-cross-linked matrix production ensured its capacity for fast wet wound sealing and good tissue fusion and integration.[40]

On the other hand, the water-loving gelatin gels are unsuitable for holding incompatible hydrophobic drugs, which is the primary disadvantage of conventional hydrogel scaffolds in drug delivery.[41−47] But unfortunately, many drugs currently used or effective in disease therapy are hydrophobic. Recent progress has been made with supramolecular hydrogels using a natural oligosaccharide, cyclodextrin (CD).[48−52] Strategies for CD incorporation into hydrogel networks include chemical or physical methods to yield either chemically or physically cross-linked networks. The unique cavity structure of CD makes it an ideal vehicle for the delivery of active ingredients into target tissues, providing sustained and controlled release of macromolecular drugs. For example, the Moncada-Basualto research group reported that lipophilic nonhydroxylated coumarins were loaded into the hydrophobic core of β-cyclodextrin to render them with trypanocidal activity in the supramolecular hydrogels produced by an interaction between the carboxylate groups with calcium ions.[53] Ki et al. realized the rapid formation of gelatin-β-cyclodextrin hydrogels by simply blending gelatin-tyramine and oxidized CD in the presence of horseradish peroxidase. The adhesive strength was significantly improved, owing to additional covalent imine bonds between aldehyde residues of the hydrogel matrix and primary amines of the tissue. On the other hand, the hydrophobic dexamethasone could be released with 2.7-fold higher efficacy.[54] The other typical approach to adding hydrophobic domains in hydrogels includes incorporating hydrophobic aliphatic chains or aromatic rings to self-assemble with hydrophobic drugs. The Zelikin research group used to apply thiocholesterol into poly(vinyl alcohol) hydrogels for the delivery of hydrophobic drugs.[55]

In order to solve the problems mentioned above at the same time, some special groups and strategies need to be introduced into the modification process of gelatin. The well-known dual-

https://doi.org/10.1021/acsomega.4c01963
ACS Omega 2024, 9, 34413−34427

Table 1. Molecular Parameters of GelMA-*NB*NAGA and GelMA-*NB*NAGA′[a]

polymer	M_w, measured by GPC (kDa)[b]	DM[c], calculated from ^{1}H NMR	DN[d], calculated from ^{1}H NMR	DM[c], determined by TNBS assay	DN[d], determined by TNBS assay
GelMA-*NB*NAGA	72.8 ± 0.2	73.1 ± 1.7%	16.0 ± 0.9%	73.3 ± 1.8%	16.5 ± 1.1%
GelMA-*NB*NAGA′	74.3 ± 0.5	15.9 ± 0.6%	71.4 ± 2.3%	15.3 ± 0.7%	73.3 ± 2.6%

[a]Reported data are the means of three replicates. [b]Mobile phase of 0.1 N sodium nitrate. [c]DM, degree of methacrylation. [d]DN, degree of NBNAGA substitution.

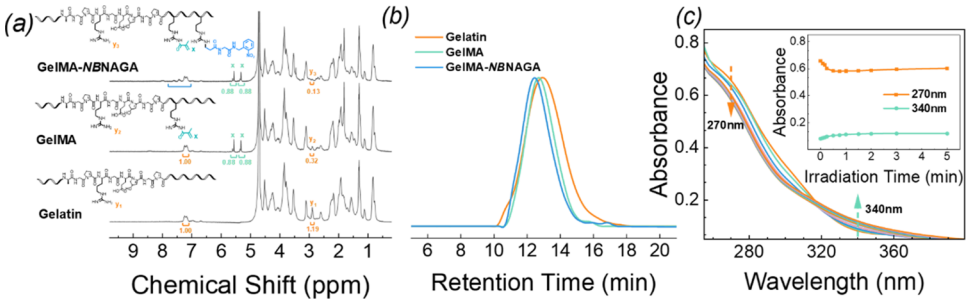

Figure 1. (a) ^{1}H NMR spectra and (b) GPC traces recorded for gelatin, GelMA, and GelMA-*NB*NAGA. (c) Time-dependent UV−vis absorbance spectra recorded for GelMA-*NB*NAGA (0.08%, w/v) in PBS upon irradiation with a 365 nm LED light (30 mW/cm^2) for varying durations (0, 0.25, 0.5, 0.75, 1, 1.5, 2, 3, and 5 min).

amide-containing monomer, *N*-acryloyl glycinamide (NAGA), has been designed for a mechanically strong supramolecular polymer hydrogel. The robust dual H-bonding microdomains were constructed in the supramolecular side chains with interactions between the C═O and N−H groups. Collectively, the similarity to the secondary structure of proteins gives rise to the critical role of the concomitant strengthening effect.[56−59] On the other hand, due to its excellent efficiency in group disintegration, *o*-nitrobenzyl (*o-NB*) is almost the best-known and most commonly used light-responsive moiety.[60] In our previous reports, it was successfully utilized as a pendant hydrophobic group of NAGA to shield the strong dual-hydrogen bonding effect of the hydrophilic dual-amide motifs, named, *N*′-(2-nitrobenzyl)-*N*-acryloyl glycinamide (*NB*NAGA).[61,62] Under 365 nm irradiation, the *o-NB* groups on side chains were released, accompanied by nitroso side products. The "uncaged" dual-amide motifs with excellent hydrophilicity, therefore, constituted the inter- or intrachain dual-hydrogen bonds besides some single hydrogen bonds, which greatly reinforced the H-bonding among side chains (Scheme 1). Thus, this class of *NB*NAGA polymers ideally served as reinforcing factors and hydrophobic drug carriers with photoinduced periodic release behavior in both intelligent *in situ*-formed polyacrylamide hydrogels and poly(ethylene glycol) supramolecular micelles. Inspired by all of the above-mentioned facts, *NB*NAGA groups were chosen to incorporate into GelMA hydrogels with respect to mechanical enhancement and hydrophobic drug delivery. It is reasonable with superiority in three aspects. First, the hydrophilic NAGA groups carrying dual-amide moieties should harden the hydrogels with dual-hydrogen-bonding interactions. Second, the hydrophobic *o-NB* groups should accommodate the hydrophobic drug *via* hydrophobic association. Third, one-step UV light stimuli facilitate both chemical cross-linking and physical cross-linking concurrently.

Herein, the simple blending of *NB*NAGA with GelMA resulted in the synthesis of a GelMA-*NB*NAGA polymer *via* Michael addition under mild conditions. Then, initiated by the hydrophilic lithium phenyl-2,4,6-trimethylbenzoylphosphinate (LAP), the GelMA-*NB*NAGA/LAP hydrogel conveniently formed under UV light irradiation, maintaining a fast gelation time within a few seconds similar to that of the GelMA/LAP hydrogel but reinforcing the gelatin-based hydrogel with superior mechanical strength. Most importantly, the excellent drug loading and controlled release capacity of hydrophobic anticancer doxorubicin (DOX) and antibiotic rifampicin (Rif) was successfully accomplished, especially for the latter on wound treatment (Scheme 1).

2. RESULTS AND DISCUSSION

2.1. Synthesis and Characterization of GelMA. Gelatin, derived from collagen, is a biocompatible and cost-effective material. Due to the relatively low melting point and instability at body temperature, a variety of hardening procedures were described in the literature.[23−25] Introduction of radically polymerizable methacrylate by a reaction with methacrylic anhydride in gelatin was first described by Schacht.[27] The more attractive concept of methacrylated gelatin (GelMA) established chemical cross-links between the protein chains in the subsequent reinforcement step. The degree of gelatin methacrylation (DM), defined as the percentage of modified ε-amino groups, was determined by 2,4,6-trinitrobenzene-sulfonic acid (TNBS) assay according to the method developed by Habeeb.[63] Results were obtained by converting the UV absorbance values at 335 nm from a glycine standard curve to amino group concentration (AC), which were 0.273 ± 0.006 and 0.073 ± 0.005 mmol/g for gelatin and GelMA, respectively. The DM of 73.3 ± 1.8% was calculated according to the AC reduction between *per* gram gelatin and GelMA samples shown in Table 1 following the equation

$$\mathrm{DM}\ (\%) = \left(1 - \frac{\mathrm{AC}_{\mathrm{GelMA}}}{\mathrm{AC}_{\mathrm{gelatin}}}\right) \times 100 \quad (1)$$

To verify the DM, proton nuclear magnetic resonance (^{1}H NMR) spectra were collected at 40 °C in deuterium oxide (Figure 1a). Baseline correction was applied before obtaining the integration values of the peaks with interest. The peak area integration values of aromatic amino acids (7.4−7.1 ppm) in

https://doi.org/10.1021/acsomega.4c01963
ACS Omega 2024, 9, 34413−34427

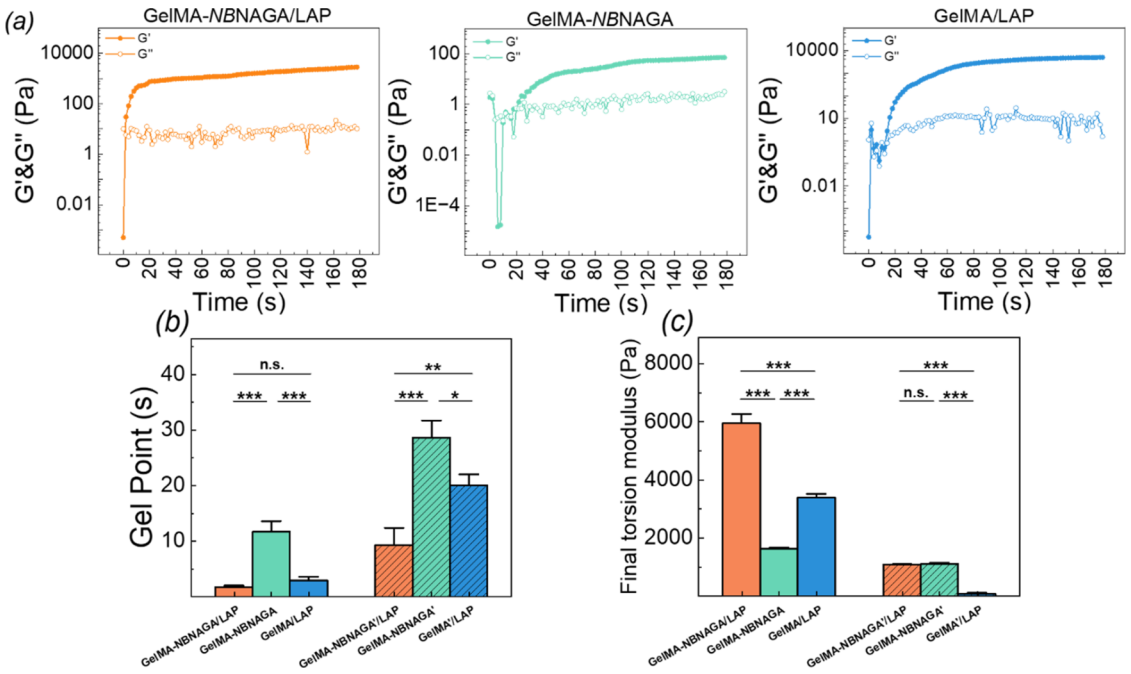

Figure 2. Mechanical characterization of the hydrogels. (a) Formation kinetics recorded from dynamic time−sweep rheological analysis of GelMA-*NB*NAGA/LAP, GelMA-*NB*NAGA, and GelMA/LAP hydrogels, respectively. (b) Gel points of different hydrogels. (c) Final storage modulus G' of different hydrogels after being stored at 4 °C for 12 h.

the gelatin (Figure 1a, bottom) and GelMA samples (Figure 1a, middle) were employed as a reference in each spectrum. The peak area integration values (PA) of lysine methylene protons appearing between 3.1 and 2.9 ppm in both gelatin and GelMA or alkene protons at 5.2 and 5.7 ppm that emerged in GelMA were used for the calculation of DM. Based on the integral ratio of y_2/y_1 or x/y_1, the DM of GelMA was calculated to be 73.1 ± 1.7% according to the current formula, which is nearly in accordance with that measured by the TNBS assay.

$$\mathrm{DM}\ (\%) = \frac{\mathrm{PA}_x}{\mathrm{PA}_{y_1}} \times 100 = \left(1 - \frac{\mathrm{PA}_{y_2}}{\mathrm{PA}_{y_1}}\right) \times 100 \tag{2}$$

The GPC trace of gelatin using DMF as an eluent (Figure 2b) revealed a monomodal elution peak with an M_w of ∼60.1 kDa. The elution peak of GelMA exhibited a clear shift to the higher molecular weight side, indicating the successful modification. However, its M_w of ∼69.1 kDa was apparently larger than 60.9 kDa calculated with ^{1}H NMR measurements and TNBS assay. It was mostly reasonable for the polarity difference after olefin modification.

Using the same method, a relatively low-level substituted GelMA′ (see Table 1) was synthesized using different reactant ratios with DM of 15.3 ± 0.7%, as determined by TNBS assay, and 15.9 ± 0.6%, as calculated from ^{1}H NMR.

2.2. Synthesis and Characterization of GelMA-*NB*NAGA. Diverse functional derivatives of natural macromolecules have been prepared *via* Michael's addition reaction under moderate conditions between unsaturated carbonyl compounds and various amines.[64] Here, we incorporated the *NB*NAGA group into the GelMA polymeric network *via* Michael addition (Scheme 1), providing the typical *o*-*NB* groups, which can be removed upon 365 nm irradiation with freshly formed dual-amide moieties enabling the modulation of the resulting biocompatible hydrogels in mechanical properties, degradation rate, porosity, and tissue adhesion. Most importantly, the functional delivery of hydrophobic drugs could be introduced into the hydrophilic hydrogels. It should be noted that due to the steric effect of the methyl group in GelMA, the neighboring double bond should not undergo Michael addition with the ε-amino group itself. On the other hand, the thorough dialysis against deionized water to remove impurities and any unreacted *NB*NAGA after the Michael addition reaction should ensure product purity. It also can be confirmed by the GPC trace of GelMA-*NB*NAGA, as shown in Figure 1b, showing a relatively monomodal and symmetric peak without an obvious shoulder at the lower or higher molecular weight side. Nevertheless, the elution peak of GelMA-NBNAGA exhibits a considerable shift to the higher molecular weight side compared with the two precursor polymers. The M_w values were determined to be 72.8 ± 0.2 kDa, as listed in Table 1.

The AC of GelMA-*NB*NAGA was 0.028 ± 0.003 mmol/g, as determined by TNBS assay, and the degree of *NB*NAGA substitution (DN) defined as the percentage of further modified ε-amino groups was 16.5 ± 1.1%, as shown in Table 1 following the equation

$$\mathrm{DN}\ (\%) = \left(1 - \frac{\mathrm{AC}_{\mathrm{GelMA}} - \mathrm{AC}_{\mathrm{GelMA\text{-}NBNAGA}}}{\mathrm{AC}_{\mathrm{gelatin}}}\right) \times 100 \tag{3}$$

Similarly, the ^{1}H NMR measurement was also carried out for the verification. The peak area integration values of alkene protons (5.2−5.7 ppm) in the GelMA (Figure 1, middle) and GelMA-*NB*NAGA samples (Figure 1, top) were employed as a reference in each spectrum. The PA reduction of lysine methylene protons at 3.1−2.9 ppm was used for DN calculation. Based on the integral ratio of $(y_2 - y_3)/y_1$, the DN of GelMA was calculated to be 16.0 ± 0.9% according to

https://doi.org/10.1021/acsomega.4c01963
ACS Omega 2024, 9, 34413−34427

the current formula, which was approximately equal to the result of the TNBS assay (Table 1).

$$\mathrm{DN}\ (\%) = \frac{\mathrm{PA}_{y_2} - \mathrm{PA}_{y_3}}{\mathrm{PA}_{y_1}} \times 100 \quad (4)$$

In the discussion above, the molecular weight of GelMA-*NB*NAGA was calculated to be ~61.6 kDa, which is normally smaller than that depicted by GPC measurement.

By varying the feeding ratio, the lower-level substituted GelMA′ was further modified by *NB*NAGA following a similar approach. The molecular parameters of the obtained product, GelMA-*NB*NAGA′, are summarized in Table 1. The DN was 71.4 ± 2.3%, as calculated from ^{1}H NMR, and 73.3 ± 2.6%, as determined by TNBS assay, and the molecular weight was calculated to be ~63.4 kDa, also much smaller than 74.3 ± 0.5 kDa measured by GPC.

Next, a 0.08% w/v GelMA-*NB*NAGA polymer solution in PBS was freshly prepared to verify the photolysis performance. Figure 1c shows the time-dependent UV−visible (UV−vis) absorbance spectra as irradiated with 365 nm light-emitting diode (LED) light (30 mW/cm^2) for varying durations. In line with our previous studies on the *NB*NAGA monomer, a PEG-*b*-P*NB*NAGA diblock copolymer, and a P(AM-*co*-*NB*NAGA) random copolymer, the characteristic absorption maximum at ~270 nm gradually decreased with irradiation time, while the absorption at ~340 nm increased. Electrospray ionization mass spectrometry (ESI-MS) analysis incorporated with high performance liquid chromatography (HPLC) measurements well confirmed the photocleavability of the released *o-NB* group accompanied by the production of a nitroso moiety.[61,62] With 30 mW/cm^2 LED light irradiation, the absorbance intensity of the GelMA-*NB*NAGA solution nearly stabilized in about 1 min, indicating that the photoinduced reaction had almost accomplished, which was much faster than ~20 min under 1.2 mW/cm^2 LED light irradiation discussed before.[62] So, in the following discussion, 3 min irradiation-induced GelMA-*NB*NAGA hydrogels were chosen for performance tests. The UV responsiveness of the GelMA-NBNAGA′ precursor solution was also characterized, inducing similar results without obvious distinction.

2.3. Hydrogel Preparation. Naturally derived material, *e.g.*, gelatin, is optimal for the fabrication of biocompatible hydrogels suitable for wound healing, while polymeric hydrogels are fascinating platforms as three-dimensional (3D) scaffolds for tissue repair and therapeutic delivery systems. Among others, GelMA hydrogels have been devoted for combining them to form a cross-linked network *via* free-radical polymerization. The tripeptide of arginyl−glycyl−aspartic acid (RGD) in GelMA favors certain cellular activities such as attachment, spreading, and so forth, which plays key roles in dermal wound healing, morphogenesis, and tissue restoration. Recent efforts on GelMA-based hydrogels were focused on incorporating bioactive and functional nanomaterials, aiming to provide enhanced physicochemical and biological properties.[37] In this study, by incorporating reactive *o*-NB groups into GelMA, a dual-photo-cross-linkable GelMA-*NB*NAGA prepolymer was synthesized.

Lin et al. demonstrated that 10% GelMA offered optimal conditions to increase the adherence and cell growth.[65] Given the insignificant change in molecular weight after group substitution, 10% GelMA-*NB*NAGA was selected as the matrix hydrogel precursor solution, which was admixed with 0.2% polymerization initiator LAP. The next was *in situ* 365 nm light irradiation for about several minutes, and the benefits of this approach were double: (i) C═C double bonds were initiated by LAP *via* free-radical polymerization to form a chemical cross-linked network and (ii) the *o-NB* groups on side chains of the GelMA-*NB*NAGA precursor polymer solution were released, and the "uncaged" dual-amide motifs with excellent hydrophilicity, therefore, constituted the interchain or intrachain dual hydrogen bonds besides some single hydrogen bonds, which greatly reinforced the H bonding among side chains and created the second physical cross-linked network (Scheme 1). Thus, a chemical and physical dual-cross-linked GelMA-*NB*NAGA/LAP hydrogel patch could form through on-step ultraviolet cross-linking. For comparison, the chemical single-cross-linked GelMA/LAP hydrogels and physical single-cross-linked GelMA-*NB*NAGA hydrogels were prepared comparably following the same protocol. Furthermore, GelMA-*NB*NAGA′/LAP, GelMA-*NB*NAGA′, and GelMA′/LAP hydrogels were also fabricated with a comparatively lower DM and higher DN.

2.4. Rheological and Mechanical Properties. To track the gelation process, an *in situ* dynamic time−sweep rheological experiment was carried out with a 365 nm ultraviolet light source using a radiation intensity of 30 mW/cm^2. As shown in Figure 2a, the hydrogels were rapidly formed in a few seconds, and the values of G' and G'' tended to be stable after tens of seconds, demonstrating the rapid gelation ability of the system and the integrity and stability of the network. However, there was a significant difference among diverse hydrogels whether they contained *NB*NAGA modification and LAP addition or not. The gel points were achieved at 1.7 ± 0.3 s for GelMA-*NB*NAGA/LAP hydrogels, slightly faster than those at 2.9 ± 0.4 s for GelMA/LAP hydrogels. Nevertheless, these are much faster than the 11.7 ± 1.9 s for GelMA-*NB*NAGA hydrogels without LAP (Figure 2b). These results indicate that the UV-induced dual-cross-linked structure of chemically cross-linked GelMA hydrogels and uncaged physical H-bonding in GelMA-NBNAGA/LAP ones accelerated the gelling process, especially for comparison with individual physical networks caused by *o-NB* group separation in GelMA-*NB*NAGA hydrogels. Moreover, the increase in the storage modulus, G', gradually reached the plateau in about 1 min, which is in accordance with the variation time observed in UV absorbance analysis.

A similar situation occurred in the GelMA-*NB*NAGA′ system, and the gel points were 7.1 ± 0.5, 22.1 ± 2.1, and 17.5 ± 2.0 s for GelMA-*NB*NAGA′/LAP, GelMA-*NB*NAGA′, and GelMA/LAP hydrogels, respectively, which are also shown in Figure 2b. Generally, compared with the GelMA-*NB*NAGA system, the gelation time exceeded for a few seconds, most probably due to the relatively lower DM despite higher DN, which was rationally because the chemical cross-linking was faster than the physical structuring.

The Schacht research group demonstrated that apart from the polymer or initiator concentration, degree of substitution, and UV irradiation parameters, the rheological properties of the gelatin-based hydrogels can also be controlled by the storage time.[27] Beyond the gel point, its rigidity continues to increase with increasing cross-linking density by an increase of the helix size or by lateral aggregation, leading to extended junction zones. So, after complete gelation, the final storage modulus G' was described uniformly behind storage at 4 °C for 12 h. Figure 2c represents the final G' of 5958 ± 316 Pa for

https://doi.org/10.1021/acsomega.4c01963
ACS Omega 2024, 9, 34413−34427

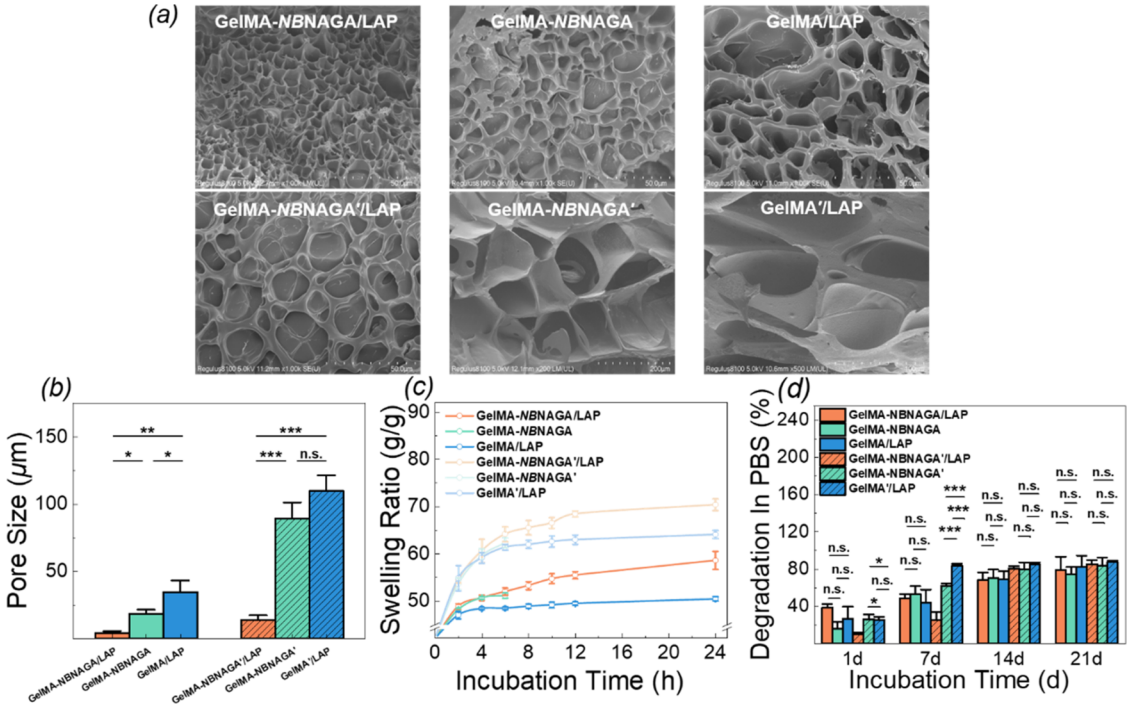

Figure 3. Pore characteristics, swelling ratios, and *in vitro* degradation properties. (a) Representative SEM images, (b) pore size characterization, (c) swelling ratios in PBS, and (d) degradation properties in PBS of different hydrogels.

GelMA-NBNAGA/LAP hydrogels, much larger than those of 3394 ± 123 Pa for GelMA/LAP hydrogels and 1643 ± 35 Pa for GelMA-NBNAGA without LAP, which exhibited the uniformed comparison with gelation time duration. These results indicate that the dual-network structure of UV-cross-linked GelMA and UV-uncaged H-bond interaction greatly strengthened the hydrogel, primarily by increasing the degree of internal cross-linking.

However, it was worth noting that the final storage modulus G' was 1107 ± 47 Pa for GelMA-*NB*NAGA′ hydrogels without LAP, a bit higher than that of 1092 ± 12 Pa for GelMA-NBNAGA′/LAP hydrogels (Figure 2c). It has been reported that the formation of chemical bonds during UV exposure will further restrict or limit physical structuring.[27] When DM is high, such as above 70% for the GelMA-*NB*NAGA/LAP hydrogel, the chemical network dominated and the slow process of physical cross-linking further strengthened the hydrogels. On the contrary, as the DN was high, such as above 70% for the GelMA-*NB*NAGA′/LAP hydrogel, the physical cross-linking dominated, and the fast process of chemical cross-linking constituted ahead would probably limit the physical structuring. In addition, due to the lower DM of ∼15% without DN, the G' values of GelMA′/LAP hydrogels with a single chemical cross-linking network were the lowest ones of 84 ± 13 Pa. The substitution degree of DM and DN dependence on mechanical properties will be analyzed in the next study.

2.5. Porosity, Swellability, and *In Vitro* Degradation. A scanning electron microscope (SEM) was used to observe the detailed structure of GelMA-*NB*NAGA/LAP, GelMA-*NB*NAGA, and GelMA/LAP hydrogels at the micrometer scale (Figure 3a). Clearly, the hydrogels formed were porous, and the observed average pore sizes were 4.3 ± 1.4, 18.5 ± 3.0, and 34.6 ± 8.7 μm, respectively. GelMA-*NB*NAGA/LAP hydrogels had the smallest pores and densest structures, in accordance with the results of mechanical testing. A contrastive observation for different DM and DN of GelMA-*NB*NAGA′/LAP, GelMA-*NB*NAGA′, and GelMA′/LAP hydrogels was also shown. Generally, the larger average pore sizes were obtained with 13.8 ± 3.4, 89.1 ± 12.2, and 109.8 ± 11.7 μm, respectively. However, undesirable results inconsistent with their mechanical analysis emerged. Although GelMA-*NB*NAGA′ hydrogels had a little advantage on G' than GelMA-NBNAGA′/LAP hydrogels, the pore characteristics of dual-cross-linking inherent in GelMA-*NB*NAGA′/LAP hydrogels were shown with more compact structures than single-cross-linking inside GelMA-*NB*NAGA′ hydrogels. It should be noted that the lyophilization prior to SEM measurement could affect the apparent porosity of these hydrogels.[66]

Throughout 24 h of incubation in PBS at 37 °C, changes in the mass of different hydrogels were recorded, and the swelling ratios (SRs) were determined at various time points. Our results demonstrated that the hydrogels with dual-cross-linked network showed increasingly higher SRs of 58.6 ± 1.9 g/g for GelMA-*NB*NAGA/LAP hydrogels and 70.4 ± 1.2 g/g for GelMA-*NB*NAGA′/LAP hydrogels (Figure 3c). The single physical cross-linked network of GelMA-*NB*NAGA and GelMA-*NB*NAGA′ hydrogels disintegrated in 6 h. The single chemical cross-linked hydrogels reached their maximum SRs after 24 h, corresponding to 50.5 ± 0.4 g/g for GelMA/LAP hydrogels and 64.1 ± 0.8 g/g for GelMA′ /LAP hydrogels, which were both unexpectedly lower than those of dual-cross-linked hydrogels, most probably due to the excellent hydrophilicity of a large number of dual-amide moieties in the latter. However, the reduced swellability of hydrogels with higher DM and lower DN could potentially enhance their adhesive properties *in vivo* for enhanced structural stability in physiological environments, sustained mechanical performance, and long-lasting tissue interactions.[67]

https://doi.org/10.1021/acsomega.4c01963
ACS Omega 2024, 9, 34413−34427

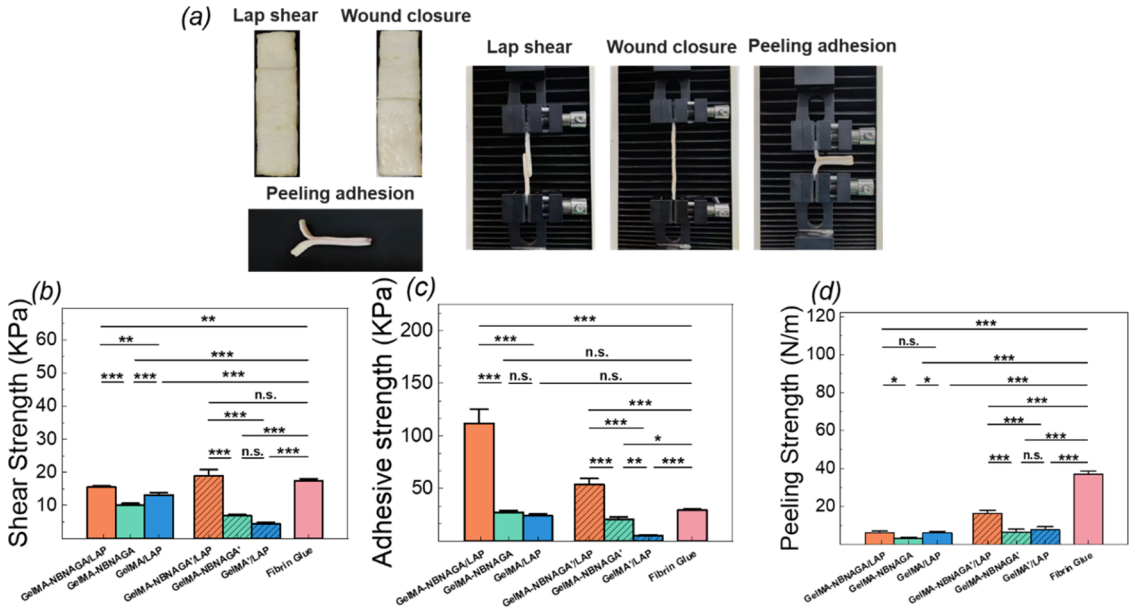

Figure 4. Adhesion properties of different hydrogels. (a) Mechanism of the adhesive study of lap shear, wound closure, and peeling adhesion used porcine skin for the study. (b) Shear strength, (c) adhesive strength, and (d) peeling strength of hydrogels and the commercially available fibrin glue.

Controlled degradation in wet environments is another technical advantage of hydrogels used for wound closure. Therefore, we aimed to investigate the *in vitro* degradation of GelMA-*NB*NAGA/LAP, GelMA-*NB*NAGA, and GelMA/LAP hydrogels at 10% w/v polymer concentrations shown in Figure 3d. Similar measurements of different samples with lower DM and higher DN values were also depicted. These hydrogel samples were all excised for the assay at days 1, 7, 14, and 21. Overall, the mass of all of the samples decreased with time after postincubation as the hydrogel degraded. For GelMA-NBNAGA/LAP hydrogels, the proportion of degradation after 7 days was 48.7 ± 4.2%, after 14 days, this had increased to 68.2 ± 8.1%, and after 21 days, 78.8 ± 14.5% degraded. These results indicate that the hydrogel progressively biodegrades. It should be noted that although the single physical cross-linked network hydrogels of GelMA-NBNAGA and GelMA-NBNAGA′ disintegrated in 6 h, the mass after lyophilization could be weighed approximately, indicating the biodegradation characteristics.

2.6. Adhesive Properties of Hydrogels. As superior tissue adhesives, a hydrogel has been the alternative strategy for sutureless wound closure to conventional methods associated with surgical procedure simplification, patient care, prognosis improvement, and localized biocidal agents. Thus, the adhesive properties of different single or dual cross-linked hydrogels were characterized in terms of lap shear, tensile, and peel tests (Figure 4a).[68] These tests were performed using standardized testing methodologies from the American Society for Testing and Materials (ASTM) in a uniaxial tensile test machine, and three selected formulations were tested. Fibrin glue was used as a control, and a total of 10 samples for each group were tested. Generally speaking, the UV-triggered dual cross-linked hydrogels of GelMA-*NB*NAGA/LAP and GelMA-*NB*NAGA′/LAP showed better adhesive properties with larger average adhesive strength than single chemical cross-linked hydrogels of GelMA/LAP and GelMA′/LAP or single physical cross-linked ones of GelMA-*NB*NAGA and GelMA-*NB*NAGA′.

The lap shear strength of gelatin hydrogels prepared from chemical or physical networks was calculated according to the ASTM F2255-05 standard. The shear strength of GelMA-NBNAGA/LAP hydrogels was 15.4 ± 0.5 kPa, higher than 10.2 ± 0.4 kPa of physical GelMA-NBNAGA hydrogels and 13.2 ± 0.7 kPa of chemical GelMA/LAP hydrogels at a 10% w/v final polymer concentration, as shown in Figure 4b. Moreover, the values were close to those observed for fibrin glue (17.5 ± 0.5 kPa). Our results also show that modification of the substitution degree on gelatin enhanced the adhesive properties of the resulting hydrogels. For example, the shear strength of GelMA-*NB*NAGA′/LAP hydrogels increased to 18.9 ± 1.9 kPa, which is higher than that of fibrin glue.

In vitro wound closure tests on native tissue of porcine skin using the ASTM F2458-05 standard were performed to characterize the ability of hydrogels to seal wound boundaries upon tensile stress. The adhesive strength obtained for chemical and physical dual-cross-linked GelMA-*NB*NAGA/LAP hydrogels at a 10% w/v polymer concentration was 111.9 ± 13.5 kPa, significantly larger than that observed for fibrin glue (29.5 ± 1.0 kPa) (Figure 4c). The hydrogels of GelMA-*NB*NAGA without LAP and GelMA with LAP processed the adhesive strength of 27.1 ± 2.0 and 24.1 ± 1.8 kPa, approximately being equal to those of fibrin glue. Concurrently, the samples with different substitution degrees had some effect on the adhesive strength. For instance, the strength of GelMA-NBNAGA′/LAP (53.8 ± 5.9 kPa) greatly decreased due to the different DM & DN, but obviously greater than those of fibrin glue and GelMA-NBNAGA′ without LAP (20.7 ± 2.3 kPa) and GelMA′ with LAP (5.3 ± 0.8 kPa).

A further class of adhesive strength tests is peeling adhesion resistance tests, and the results are shown in Figure 4d. As compared with the commercialized fibrin glue, the peeling strength of modified gelatin hydrogels was relatively smaller. Considering the advantages of gelatin with low cost and no risk for blood-related diseases, the formulations we developed might have the potential to replace fibrin glue in these applications.

https://doi.org/10.1021/acsomega.4c01963
ACS Omega 2024, 9, 34413−34427

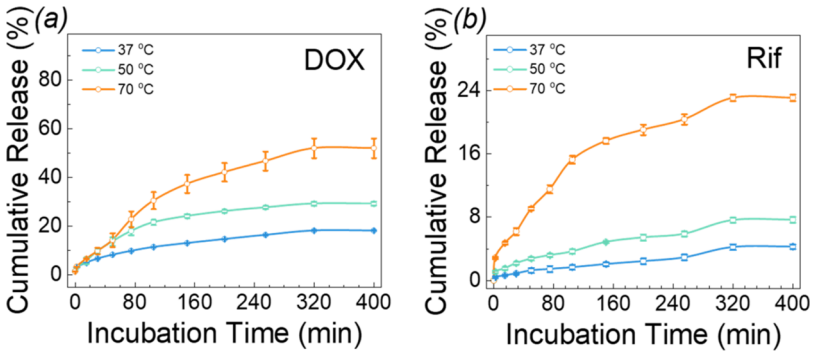

Figure 5. *In vitro* release profiles and release extent after 400 min incubation of DOX (a) and Rif (b) from the drug-loaded GelMA-NBNAGA/LAP hydrogel under varying temperatures.

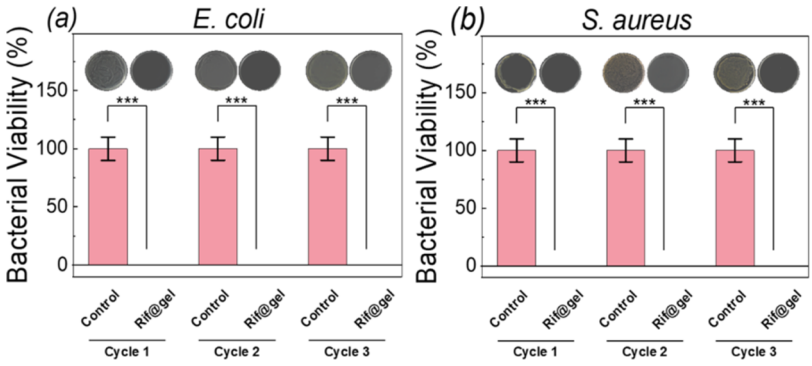

Figure 6. *In vitro* antibacterial analysis of the hydrogels. Relative bacterial viability of (a) *E. coli* and (b) *S. aureus* incubated with or without the Rif-loaded GelMA-*NB*NAGA/LAP hydrogel (Rif@gel). Also shown inside are their Images of agar plates with *E. coli* and *S. aureus* suspensions.

2.7. *In Vitro* Drug Release Behavior. As is known to all, hydrogels possess a large amount of water. So, it is problematic to render the encapsulation and release of hydrophobic drugs for their hydrophilic nature. Phase separation between encapsulated hydrophobic drugs and the hydrogel may also result in deterioration of the stability and strength of the hydrogel. The introduction of the binding sites for hydrophobic drugs promotes the development of hydrogels with the typical approaches of copolymerizing hydrophobic monomers or incorporating hydrophobic molecules. Here, the photosensitive *o-NB* groups were conveniently imported into the natural gelatin network through the Michael addition reaction and served as the hydrophobic domains. In our previous study, the photoreactive monomer, the *NB*NAGA group, was introduced to modify the polyacrylamide hydrogel for UV light responsiveness.[61,62] Surprisingly, the inclusion of the hydrophobic *o-NB* groups into hydrogels was advantageous in embedding therapeutics and controlled release of encapsulates periodically, such as the anticancer drug doxorubicin (DOX). The drug was released stepwise from the DOX-loaded hydrogel upon successive photoirradiation and heating due to the UV light-induced cleavage of *o-NB* groups and the temperature-induced weakness of "uncaged" dual hydrogen bonding, respectively.

First, DOX was chosen to be loaded into the GelMA-*NB*NAGA/LAP precursor solution due to the hydrophobic association with the aromatic nucleus in the modified side chains of gelatin. Figure 5a shows the DOX *in vitro* release profile with incubation time under different temperatures. At a body temperature of 37 °C, the cumulative release amount of DOX was rapidly increased within the incubation of ∼100 min, successively with a gentle increase to 18.2 ± 0.1% at 320 min. Probably due to the relatively more compact chemical cross-linking, the DOX release speed was slightly slower than the *NB*NAGA-modified polyacrylamide hydrogel matrix of ∼75 min reported previously, but with an almost similar cumulative release amount.[62] It is much more critical that the DOX release profile that was severely dependent on the temperature, which confirmed that the physical cross-linking originated from single and dual hydrogen bonding. The cumulative release extent was 29.3 ± 0.8 and 52.1 ± 4.0%, after 400 min incubation at 50 and 70 °C, respectively.

Rifampicin (Rif) is the model hydrophobic antibiotic used to treat tuberculosis as well as other mycobacterial diseases.[69,70] Especially, Rif is a semisynthetic fungicide and an antimicrobial agent that has bactericidal and bacteriostatic effects on skin tissues, which is significant for wound healing. The encapsulation of Rif was fabricated *via* a cosolvent self-assembly approach as a Rif@GelMA-*NB*NAGA polymer. To confirm the presence of Rif, the Rif-loaded GelMA-NBNAGA/LAP hydrogels were soaked in a PBS medium, and the UV absorbance intensity at 480 nm was monitored. Figure 5b exhibits the *in vitro* release profiles of Rif from Gel-*NB*NAGA/LAP hydrogels at 37, 50, and 70 °C. Similar to those of DOX, the cumulative release amount of Rif initially increased with the incubation time gradually and then reached a plateau at 4.3 ± 0.3, 7.7 ± 0.4, and 23.1 ± 0.4%, respectively.

2.8. *In Vitro* Antibacterial Assessment. Because of the excellent anti-inflammatory action, hydrophobic Rif was incorporated into GelMA-*NB*NAGA/LAP hydrogels *via* a cosolvent self-assembly approach. *In vitro* antimicrobial tests were performed to evaluate the antibacterial activity against Gram-negative (*Escherichia coli*) and Gram-positive (*Staphylococcus aureus*) bacteria. Figure 6a displays the agar-plate

https://doi.org/10.1021/acsomega.4c01963
ACS Omega 2024, 9, 34413−34427

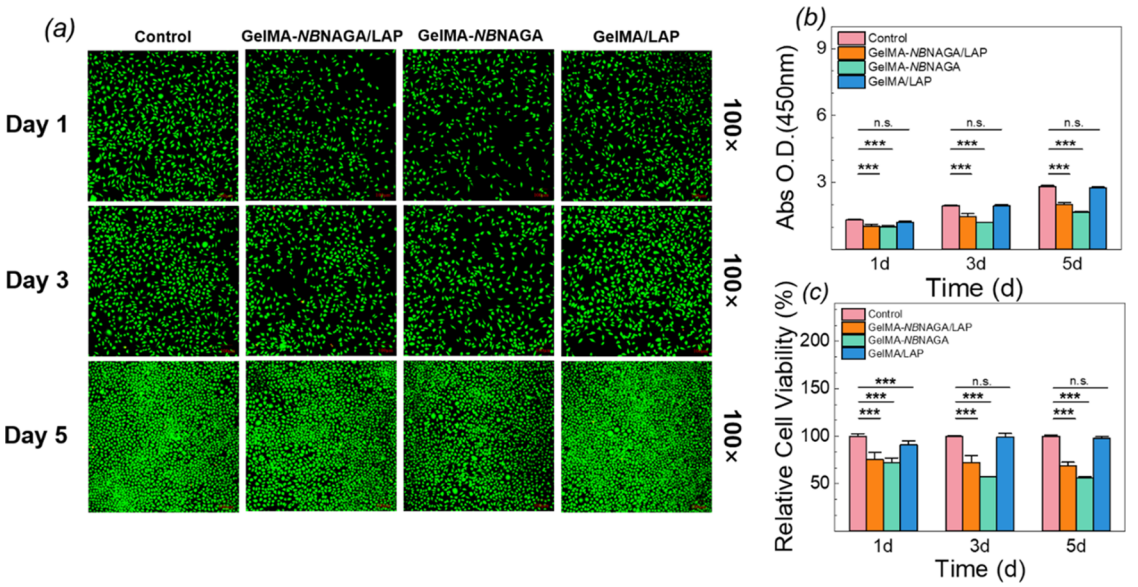

Figure 7. (a) Representative pictures of control, GelMA-*NB*NAGA/LAP, GelMA-*NB*NAGA, and GelMA/LAP hydrogels taken by a confocal laser microscope after staining with a Live/Dead Kit for 1, 3, and 5 days. (b) OD value and (c) relative cell viability of different groups at 450 nm after incubating with a CCK-8 Kit.

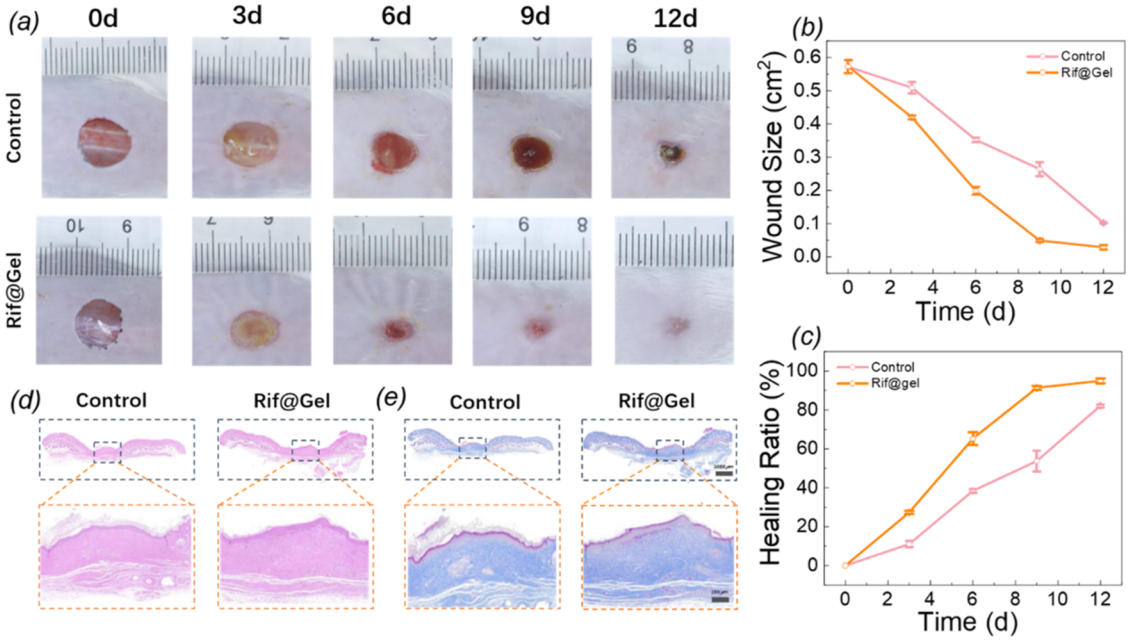

Figure 8. *In vivo* assessment of hydrogels for wound healing. (a) Digital images showing temporal development of wounds, (b) wound size in mice, and (c) wound-healing rates after treatment with and without the Rif-loaded GelMA-*NB*NAGA/LAP hydrogel (Rif@gel) on days 0, 3, 6, 9, and 12. (d) H&E staining and (e) Masson's trichrome staining of the wound section on day 18.

cultures and relative bacterial viabilities of *E. coli* incubated with or without the Rif-loaded GelMA-*NB*NAGA/LAP hydrogel (Rif@gel) for 24 h. The agar plates showed scant to no colony growth cultured by Rif@gel with respect to robust bactericidal activity without any treatment. The relative *E. coli* bacterial viability was nearly 100% without incubation for the cloudy appearance. On the contrary, nearly 100% antibacterial rates against *E. coli* bacteria were realized. Moreover, the successive two antimicrobial tests following the first step, named cycles 2 and 3, suggested sustained excellent antibacterial activity. *S. aureus* showed the same trend as that shown by *E. coli*, which is shown in Figure 6b. These results indicated that the Rif@GelMA-*NB*NAGA/LAP hydrogel exhibited excellent capability against typical bacteria, which could be ascribed to the excellent capability for drug load and release of the substituted hydrophobic *o-NB* groups mostly secreted within gelatin hydrogels.

2.9. *In Vitro* Cytocompatibility of Hydrogels. It is essential for hemostatic adhesives with favorable biocompatibility. To evaluate the cytocompatibility of different hydrogels prepared from GelMA or GelMA-*NB*NAGA polymers, live/dead assays were performed by coincubation with L929 fibroblastic cells. As shown in Figure 7a, during the whole period, a large proportion of living cells was observed through

https://doi.org/10.1021/acsomega.4c01963
ACS Omega 2024, 9, 34413−34427

a confocal laser microscope after staining with a Live/Dead Kit in the three groups of dual-cross-linked GelMA-*NB*NAGA/LAP and single-cross-linked GelMA-*NB*NAGA and GelMA/LAP hydrogels. A more careful observation demonstrated that compared with the control group and GelMA/LAP groups, the living cells of the dual-cross-linked GelMA-*NB*NAGA/LAP group were slightly decreased after incubation for 1, 3, and 5 days. It is probably rational for the physical polarity and the chemical structure of the substituted groups on gelatin and the nitroso side product accompanied by the photocleavability, which was more obvious in single-cross-linked physical hydrogels of GelMA-*NB*NAGA.

Quantification data were obtained using the Cell Counting Kit 8 (CCK-8) to further assess the cytocompatibility of the materials. The OD values among the three groups are illustrated in Figure 7b, which clearly increased with the coincubation time. The relative cell viability of GelMA-*NB*NAGA/LAP hydrogels was calculated to be 75.6 ± 7.4, 72.2 ± 7.4, and 68.8 ± 3.7% after incubation for 1, 3, and 5 days, respectively. These results suggested that hydrogels exhibited slight toxicity with barely satisfactory biocompatibility without causing many side effects in terms of cell growth and proliferation and could be expected to be used *in vivo* for further biological applications.

2.10. *In Vivo*-Infected Wound Healing of Hydrogels. To evaluate the efficiency of hydrogels in promoting wound healing, a full-thickness cutaneous wound model with *S. aureus* infection was fabricated. The *in vivo* testing was conducted on 6 male Balb/c mice, which were randomly divided into two groups: the control group with no treatment and the Rif@gel group with Rif-loaded GelMA-*NB*NAGA/LAP hydrogel treatment. Utilizing a digital camera, the entire wound-healing process was monitored, with images shown in Figure 8a. The yellow pus was clearly observed at the wound site of the control group on day 3, and the injured area appeared brightly red on day 6, indicating that the damaged site was undergoing inflammation (Figure 8a, top). Nevertheless, in the Rif@gel group, there was little yellow pus on day 3, and almost no inflamed red was discovered during the therapeutic period. Moreover, the accelerated wound closure was found generally due to the well-controlled *S. aureus* inflammation (Figure 8a, bottom). On day 3, the wound size of mice with Rif @gel treatment was deduced from 0.57 ± 0.02 to 0.42 ± 0.01 cm^2, and the healing rate was ∼27%, which are calculated and plotted in Figure 8b,c. After 6, 9, and 12 days of treatment, the wound sizes of the Rif@gel group mice were 0.20 ± 0.01, 0.049 ± 0.005, and 0.029 ± 0.007 cm^2, corresponding to the healing rates of ∼65, ∼91, and ∼94%, respectively. However, ∼18% of the wounds remained unhealed with no treatment but covered with epidermal tissue on day 12, which was not completely cured until ∼18 days of treatment. Pathological examinations of the healed wound on day 18 in the control group and the Rif@gel group are shown in Figure 8d,e, with hematoxylin and eosin (H&E) staining and Masson's trichrome staining, respectively. Except for some unshed scab tissue and few regenerated collagens in the control group, the defective skin was healed completely.

3. CONCLUSIONS

In this work, we introduce a physical and chemical dual-cross-linked network-reinforced gelatin-based hydrogel adhesive along with antibiotic on-demand delivery for the treatment of nonhealing infected wounds. A GelMA-*NB*NAGA polymer was first synthesized under moderate conditions *via* Michael addition between unsaturated alkene moieties of *NB*NAGA and ε-amino groups on GelMA. Then, 365 nm UV light-induced gelation of a GelMA-*NB*NAGA solution within a few seconds due to the combined effects of LAP-induced chemical cross-linking and *o-NB* groups uncaged physical cross-linking from the remarkable dual-hydrogen bonding of dual-amide NAGA groups. It enabled fine-tuning of various properties of hydrogels, including mechanical properties, degradation, swellability, porosity, and adhesive properties, generally superior to commercially available tissue adhesives. Most importantly, the GelMA-*NB*NAGA/LAP hydrogels were proven to support the growth, spread, and proliferation *in vitro* and further efficiently promote wound healing with the help of Rif release when wrapped up in the mice model. Taken together, the GelMA-*NB*NAGA/LAP bioactive hydrogels can promote skin wound healing in a simple, economical, effective, and safe manner.

4. EXPERIMENTAL SECTION

4.1. Materials. Gelatin from porcine skin (type A), 2,4,6-trinitrobenzenesulfonic acid (TNBS), methacrylic anhydride (MA), lithium phenyl-2,4,6-trimethylbenzoylphosphinate (LAP), rifampicin (Rif), and doxorubicin hydrochloride (DOX·HCl) were purchased from Sigma-Aldrich Reagent (Shanghai, China) and used directly without purification. Photoreactive monomer *N*′-(2-nitrobenzyl)-*N*-acryloyl glycinamide (*NB*NAGA) was synthesized through the esterification of *N*-acryloylglycine with 2-nitrobenzyl amine as reported previously.[61] PBS was obtained from Dalian Bergolin Biotechnology Co., Ltd. Water was deionized with a Milli-Q SP reagent water system (Millipore) to a specific resistivity of 18.4 MΩ·cm. Dimethyl sulfoxide (DMSO) was dried over calcium hydride (CaH_2) and vacuum-distilled just before use. All other reagents were commercial chemicals and used as received, unless otherwise specified.

4.2. Synthesis of GelMA. GelMA was synthesized following the literature.[40] Briefly, after complete dissolution of 10% w/v type A gelatin in PBS at 60 °C for 30 min, 0.62 mL of methacrylic anhydride (MA) per gram of gelatin was added to the gelatin solution at a rate of 0.5 mL/min with continuous stirring. The mixture could react at 50 °C for 2.5 h followed by dilution with 100 mL of PBS and dialysis against deionized water using membranes (MWCO 8000−14,000) for 7 days at 40 °C to remove unreacted MA and any byproducts. After sterile filtration and lyophilization for 2 days, GelMA was stored at −80 °C until further use. The DM was verified by TNBS assay and ^{1}H NMR measurement, respectively.

4.3. Synthesis of GelMA-*NB*NAGA. *NB*NAGA (0.6680 g, 2.53 mmol) was weighted into a transparent vial equipped with a magnetic stir bar, and 13.32 mL of DMSO was then added, which was heated to 60 °C in an oil bath for 3 h. On the other hand, 1.3320 g of GelMA was added into 13.32 mL of water and stirred for 3 h at 50 °C followed by adjustment to pH 8−9 with saturated $NaHCO_3$ and air bubble removal. The DMSO solution of NBNAGA was added dropwise, and the mixture was stirred in an oil bath at 50 °C for 24 h. After dialysis (MWCO 3500) for 72 h to remove the unreacted monomer and freeze-drying for 24 h, the white foamy substance was obtained as GelMA-*NB*NAGA, and stored at −20 °C for the next preparation of hydrogels. The DN was calculated by TNBS assay and ^{1}H NMR measurement, respectively.

https://doi.org/10.1021/acsomega.4c01963
ACS Omega 2024, 9, 34413−34427

4.4. Polymer Characterization. All of the nuclear magnetic resonance (NMR) spectra were acquired on a 400 MHz Bruker Ascend Aeon 400 instrument (resonance frequency: 400 MHz for ^{1}H). The molecular weights were determined by PL-GPC50 gel permeation chromatography (GPC), which was equipped with a differential refractive index detector and used two PL aquagel−OH mixed-M columns (8 μm, 7.5 mm × 300 mm) at an oven temperature of 40 °C. The eluent was 0.2 M $NaNO_3$ mixed with 0.01 M NaH_2PO_4 (pH7), and a variety of standard samples of dextran (538,000, 128,800, 68,900, 28,230, 15,190, 3860, 1470) were employed for calibration. The fluorescence spectra were acquired on a Fluoaromax-plus spectrofluorometer (HORIBA). The UV−vis absorbance spectra were recorded on a TU-1910 double-beam UV−vis spectrophotometer (Puxi General Instrumental Company, China).

4.5. Hydrogel Preparation. For hydrogels of GelMA-*NB*NAGA/LAP, the freeze-dried GelMA-*NB*NAGA foams were dissolved in a PBS solution at 40 °C with a concentration of 10% w/v, and then 0.2% w/v LAP was added as a photoinitiator. For hydrogels of GelMA-*NB*NAGA, the freeze-dried GelMA-*NB*NAGA foams were dissolved in a PBS solution at 40 °C with a 10% w/v concentration without LAP. For the hydrogel precursor of GelMA/LAP, the freeze-dried GelMA foams were dissolved in a PBS solution at 40 °C with a 10% w/v concentration, and then 0.2% w/v LAP was added. The mixture solution was transferred into a mold of PTFE, and irradiated with an ultraviolet lamp (LG-3535, AC90-240 V, 50 Hz, 18W, Shenzhen Lianhuicheng Technology Co., Ltd.) under 365 nm LED light (30 mW/cm^2) for 3 min in a completely dark environment; the hydrogels GelMA-*NB*NAGA/LAP, GelMA-*NB*NAGA, and GelMA/LAP were obtained at room temperature. A similar protocol was employed for the preparation of GelMA-*NB*NAGA′/LAP, GelMA-*NB*NAGA′, and GelMA′/LAP hydrogels.

4.6. Rheological Behavior of Hydrogels. The rheological properties were characterized by a rotary rheometer (Anton Paar MCR 302e). The experiments were carried out on a parallel plate (25 mm diameter) geometry. The stiffness of these hydrogels was measured by a time−sweep test with a constant strain of 1%, a frequency of 1 Hz, and a 0.5 mm clearance at 25 °C. The gel point was determined at the time when the storage modulus (G') surpassed the loss modulus (G''). The stability of these hydrogels cured at 4 °C for 24 h was measured by a frequency sweep test with a constant strain of 1% and changing the frequency from 0.1 to 100 rad/s at 25 °C.

4.7. Scanning Electron Microscopy (SEM) Analysis. SEM imaging was performed on a Hitachi Regulus 8100 field emission scanning electron microscope (SEM) examining the gross morphology and porosity of hydrogels after spraying a thin gold film on the freeze-dried sample. The porosity and pore sizes of hydrogels were averaged from at least 3 images from 3 samples for each condition by using ImageJ software (n = 5).

4.8. Evaluation of the *In Vitro* Swelling Ratio and Degradation. The swelling ratio (SR) was determined by incubation in PBS at 37 °C for 24 h. Samples were then lightly blotted dry for W_s. Their dried weights W_d were measured after lyophilizationn. The SR of the swollen gel was calculated according to the following equation

$$SR = \frac{W_s - W_d}{W_d} \quad (5)$$

To evaluate the degree of *in vitro* degradation, hydrogels were freeze-dried, weighed, and placed in a 24-well plate with 2 mL of PBS solutions at 37 °C for 3 weeks. The PBS solutions were refreshed every 3 days. On days 1, 7, 14, and 21 postincubation, the samples were freeze-dried and weighed (n = 5).

4.9. Adhesion Study. Lap shear, tensile, and peel tests were performed by using porcine skin as a model. The respective tests were based on modified ASTM F2255, ASTM F2458, and ASTM F2256 protocols. A tensile meter (WD-100) equipped with a 100 N load cell was used to study the adhesive properties of the prepared formulations. All mechanical tests were performed at a tensile rate of 5 mm/min. Porcine skins were purchased from a local slaughterhouse immediately after their death. Dry porcine skin substrates were cut into pieces with an area of 1.5 × 5 cm^2 and rehydrated for 1 h in PBS at 37 °C. During the lap shear step, a freshly prepared precursor solution was first added to one end of the inner surface of the skin (∼500 μL), and the hydrogel formed by UV irradiation. Another solution was applied to the other surface and added to the previous one to generate an overlapping area of 2 × 1.5 cm^2. The area of the substrate overlap was measured by using digital calipers immediately before testing. A weight of 100 g pressure was applied for 30 min to enhance adhesion. The sealant shear strength was determined at the point of detachment. As for the tensile test, precursor hydrogel solutions (∼500 μL) were injected into the desired adhesion zone (15 × 3.5 mm^2) and cross-linked by UV. The maximum adhesive strength of each sample was obtained at the point of tearing. For the peeling adhesion test, one end of the porcine skin was kept open to limit deformation at the crack tip. Then, precursor hydrogel solutions (∼500 μL) were injected on the membrane surface (4 × 1.5 cm^2) and a hydrogel polymerized by UV irradiation. Finally, another porcine skin was bonded, forming a bilayer with an edge crack. All measurements were repeated 3 times.

4.10. *In Vitro* Release of DOX from the Hydrogels. For the encapsulation of DOX, the DOX·HCl solution with a concentration of 0.5 g/L was first prepared. Then, 0.0200 g of GelMA-*NB*NAGA was dissolved in the mixture of 0.18 mL of a DOX·HCl solution at 40 °C, and the photoinitiator was added to a final LAP concentration of 0.2% w/v. After careful vibration to drive away excess bubbles, the mixture was transferred to a cylindrical mold with an inner diameter of 10 mm and a height of 2 mm. After being irradiated under 365 nm LED light (30 mW/cm^2) for 3 min in a completely dark environment, the obtained hydrogel was added in an instant into 15 mL of deionized water under gentle shaking at 37 °C. At selected time intervals, aliquots of the external medium were withdrawn and replaced with the same volume of a fresh buffer solution. The DOX concentrations in the dialysates were determined by measuring the fluorescence intensity of DOX at 595 nm (λ_{ex} = 480 nm) against the standard calibration curve. The cumulative amount of release amounts was obtained by a further calculation, and the percentages of DOX release were plotted against time. For comparison, similar tests also applied at 50 and 70 °C, respectively.

4.11. Antimicrobial Rif Release Studies. The encapsulation of Rif was fabricated *via* a cosolvent self-assembly approach. Typically, 0.2000 g of GelMA-*NB*NAGA was

https://doi.org/10.1021/acsomega.4c01963
ACS Omega 2024, 9, 34413−34427

dissolved in 50 mL of a PBS solution, which was stirred at 600 rpm in a water bath at 40 °C for 2 h. Then, 0.1 g of Rif in 5 mL of DMSO was slowly added into the GelMA-*NB*NAGA solution at a rate of 0.1 mL/min. After stirring for another 24 h, the organic solvent and unloaded Rif were removed by thorough dialysis against deionized water for 24 h using a cellulose membrane (MWCO 3500). The fresh deionized water was replaced approximately every 6 h. The final dialysate was freeze-dried, and the red-foamed powder of the Rif@GelMA-*NB*NAGA polymer was obtained.

For preparation of Rif-loaded hydrogels, 0.0200 g of the Rif@GelMA-*NB*NAGA polymer was dissolved in 0.2 mL of PBS at 40 °C with a concentration of 10% w/v along with the addition of a photoinitiator with a final LAP concentration of 0.2% w/v. Then, gelation occurred under irradiation under a 365 nm LED light (30 mW/cm^2). The *in vitro* Rif release profile was obtained using a UV−vis spectroscope, and the Rif concentrations in the dialysates were determined by measuring the UV absorbance intensity at 480 nm against the standard calibration curve. Approximately, following the procedure of DOX release measurement, similar comparative tests also applied at 50 and 70 °C, respectively.

4.12. *In Vitro* Evaluation of Antimicrobial Activity. Antibacterial properties of Rif@GelMA-*NB*NAGA/LAP hydrogels (Rif@gel) were evaluated against Gram-negative (*E. coli*) and Gram-positive (*S. aureus*) bacteria. All hydrogel samples were cured by ultraviolet in 96-well plates for 30 min and then rinsed with PBS buffer. Then, 50 μL of a bacterial suspension with a concentration of 1 × 10^5 CFU/mL in tryptic soy broth (TSB) was dropped on hydrogel surfaces. After 24 h of incubation at 37 °C, the bacterial solution was collected by washing with 950 μL of PBS buffer. Then, 100 μL of the collected solution was transferred onto TSB agar plates and spread evenly. After incubation at 37 °C for another 24 h, the colony numbers of on the agar plates were examined for survival counting. Furthermore, in order to monitor the sustained antibacterial activity of the hydrogel, another 50 μL of the bacterial suspension was dropped on hydrogel surfaces successively, and a similar protocol was employed for the second 24 h incubation. After continuing the same operation twice, the results of cycles 1, 2, and 3 were obtained.

4.13. Cell Culture and Cytotoxicity Assay. Mouse fibroblast L929 cells were chosen as the models to evaluate the biocompatibility of gel. L929 cells were cultured in Dulbecco's modified Eagle medium (DMEM; Gibco) supplemented with 10% fetal bovine serum and 1% penicillin/streptomycin. For cytotoxicity assay, L929 cells were added to 96-well plates at a density of 4 × 10^6 cells/mL and incubated with the leach liquor of hydrogels. After certain periods of incubation, the CCK-8 reagent was added to 96-well plates for culturing in a 37 °C incubator with 5% CO_2 for 2 h. The cell viability and proliferation were quantified by a multimode microplate reader at 450 nm. In order to better observe the growth of cells, L929 cells were incubated with a Live/Dead reagent (Calcein-AM/PI) for 15 min at 37 °C. The fluorescence images were taken by LSCM. For each sample, five independent cultures were prepared, and proliferation assays were repeated 3 times for each culture.

4.14. *In Vivo* Wound-Healing Assay. For the wound-healing experiment, 6 male Balb/c mice were selected to evaluate the wound-healing efficiency of gels. All mice were randomly divided into 2 groups: the control group and the gel group. Namely, the control group did not undergo any treatment, except for wrapping gauze. The gel group was treated with Rif@GelMA-NBNAGA/LAP hydrogels as Rif@gels. After anesthetization with 1% pentobarbital (50 mg/kg) by intraperitoneal injection, the fur of the dorsal skin in all mice was shaved, and the remaining hair was completely removed by applying depilatory cream for 10 min. One circular full-thickness wound about 8 mm in diameter was created on the back of each rat. Subsequently, 50 μL of an *S. aureus* suspension (1.0 × 10^6 CFU/mL) was inoculated into the created wound. Hydrogel precursor solutions were prepared and added to a one-time-use syringe in advance. Then, the precursor solution was injected into the wound and spread evenly. The hydrogel was formed at the wound site by 365 nm irradiation for 3 min. Finally, the wound covered by the hydrogels was wrapped with sterile gauze. All mice were placed in individually ventilated cages to prevent mutual interference. The dressing was changed every 3 days, and pictures of the wounds were taken on days 0, 3, 6, 9, and 12 by a digital camera. The rate of wound healing in different groups was calculated according to the following formula

$$\text{healing ratio (\%)} = \frac{S_0 - S_t}{S_0} \times 100\% \quad (6)$$

Here, S_0 means the initial area of the wound and S_t means the remaining wound area at each time point.

4.15. Histopathological Study. Wound histology specimens were collected on day 18. All of the harvested samples were fixed in a 4% paraformaldehyde solution for 12 h and embedded in paraffin to prepare 5-μm-thick tissue sections. Representative specimens were stained with hematoxylin and eosin (H&E) and Masson trichrome to observe the histological images by microscopy.

4.16. Statistical Analysis. All data were presented as mean ± standard deviation (SD), based on three replicates, and repeated in at least three independent experiments. A comparison of the difference between groups was evaluated by Student's *t*-test, and considered as $^*p < 0.05$, $^{**}p < 0.01$, $^{***}p < 0.001$, $^{****}p < 0.0001$, and n.s. no significance.

AUTHOR INFORMATION

Corresponding Authors

Zhiyuan Zhu − *Taizhou Research Institute, Southern University of Science and Technology, Taizhou, Zhejiang 318001, P. R. China;* orcid.org/0000-0003-1735-0739; Email: zhu.zhiyuan@outlook.com

Jingyi Rao − *Hubei Key Laboratory of Material Chemistry and Service Failure, Hubei Engineering Research Center for Biomaterials and Medical Protective Materials, School of Chemistry and Chemical Engineering, Huazhong University of Science and Technology, Wuhan, Hubei 430074, P. R. China;* orcid.org/0000-0002-3203-1579; Email: jrao@hust.edu.cn

Jingyan Zhang − *Anhui Advanced Building Materials International Joint Research Center, School of Materials and Chemical Engineering, Anhui Jianzhu University, Hefei, Anhui 230022, P. R. China;* orcid.org/0000-0002-3495-6225; Email: zhangjy@ahjzu.edu.cn

Authors

Di An − *Anhui Advanced Building Materials International Joint Research Center, School of Materials and Chemical Engineering, Anhui Jianzhu University, Hefei, Anhui 230022, P. R. China*

https://doi.org/10.1021/acsomega.4c01963
ACS Omega 2024, 9, 34413−34427

Zhengkai Wang − *Anhui Advanced Building Materials International Joint Research Center, School of Materials and Chemical Engineering, Anhui Jianzhu University, Hefei, Anhui 230022, P. R. China*
Yishuo Ning − *Anhui Advanced Building Materials International Joint Research Center, School of Materials and Chemical Engineering, Anhui Jianzhu University, Hefei, Anhui 230022, P. R. China*
Yuxing Yue − *Anhui Advanced Building Materials International Joint Research Center, School of Materials and Chemical Engineering, Anhui Jianzhu University, Hefei, Anhui 230022, P. R. China*
Han Xuan − *Anhui Advanced Building Materials International Joint Research Center, School of Materials and Chemical Engineering, Anhui Jianzhu University, Hefei, Anhui 230022, P. R. China*
Yongjin Hu − *Hubei Key Laboratory of Material Chemistry and Service Failure, Hubei Engineering Research Center for Biomaterials and Medical Protective Materials, School of Chemistry and Chemical Engineering, Huazhong University of Science and Technology, Wuhan, Hubei 430074, P. R. China*
Mingdi Yang − *Anhui Advanced Building Materials International Joint Research Center, School of Materials and Chemical Engineering, Anhui Jianzhu University, Hefei, Anhui 230022, P. R. China*
Haiou Zhou − *Anhui Advanced Building Materials International Joint Research Center, School of Materials and Chemical Engineering, Anhui Jianzhu University, Hefei, Anhui 230022, P. R. China*
Qianqian Liu − *Anhui Advanced Building Materials International Joint Research Center, School of Materials and Chemical Engineering, Anhui Jianzhu University, Hefei, Anhui 230022, P. R. China*
Xianbiao Wang − *Anhui Advanced Building Materials International Joint Research Center, School of Materials and Chemical Engineering, Anhui Jianzhu University, Hefei, Anhui 230022, P. R. China;* orcid.org/0000-0003-3746-9163
Ping Wang − *Anhui Advanced Building Materials International Joint Research Center, School of Materials and Chemical Engineering, Anhui Jianzhu University, Hefei, Anhui 230022, P. R. China*

Complete contact information is available at: https://pubs.acs.org/10.1021/acsomega.4c01963

Author Contributions

This manuscript was written through the contributions of all authors. All authors have given approval to the final version of the manuscript.

Notes

The authors declare no competing financial interest.

■ ACKNOWLEDGMENTS

Financial support from the National Natural Scientific Foundation of China (NNSFC) Project (52003096, 21976003, and 21004001), the opening Foundation of State Key Laboratory of Organic−Inorganic Composites, Beijing University of Chemical Technology (oic-202301011), the Anhui Provincial Key Research and Development Project (2022h11020025), the Natural Science Research Project of Anhui Provincial Education Department (2023AH040037, 2022AH020024), and the Ph.D. Start-up Fund of Anhui Jianzhu University (2020QDZ06), is gratefully acknowledged.

■ REFERENCES

(1) Elias, P. M.; Ferngold, K. R. *Skin Barrier*; CRC Press, 2006.
(2) Montagna, W. *Structure and Function of Skin*; Elsevier, 2012.
(3) Dąbrowska, A. K.; Spano, F.; Derler, S.; Adlhart, C.; Spencer, N. D.; Rossi, R. M. The Relationship between Skin Function, Barrier Properties, and Body-Dependent Factors. *Skin Res. Technol.* **2018**, *24*, 165−174.
(4) Simões, D.; Miguel, S. P.; Ribeiro, M. P.; Coutinho, P.; Mendonça, A. G.; Correia, I. J. Recent Advances on Antimicrobial Wound Dressing: A Review. *Eur. J. Pharm. Biopharm.* **2018**, *127*, 130−141.
(5) Saghazadeh, S.; Rinoldi, C.; Schot, M.; Kashaf, S. S.; Sharifi, F.; Jalilian, E.; Nuutila, K.; Giatsidis, G.; Mostafalu, P.; Derakhshandeh, H.; et al. Drug delivery systems and materials for wound healing applications. *Adv. Drug Delivery Rev.* **2018**, *127*, 138−166.
(6) Nam, S.; Mooney, D. Polymeric Tissue Adhesives. *Chem. Rev.* **2021**, *121* (18), 11336−11384.
(7) Kamoun, E. A.; Kenawy, E. R. S.; Chen, X. A Review on Polymeric Hydrogel Membranes for Wound Dressing Applications: PVA-Based Hydrogel Dressings. *J. Adv. Res.* **2017**, *8*, 217−233.
(8) Kim, H. Wound Dressing Materials: The Essentials. *J. Wound Manage. Res.* **2018**, *14*, 141−142.
(9) Liu, X.; Chen, D.; Feng, S.; Yang, M.; Yang, M. Super-Stretchable Hydrogel Films with High Fracture Energy Enabled by Coordination Nanoparticles as Multifunctional Wound Dressings. *ACS Appl. Polym. Mater.* **2023**, *5* (9), 7318−7327.
(10) Ahmed, E. M. Hydrogel: Preparation, Characterization, and Applications: A Review. *J. Adv. Res.* **2015**, *6*, 105−121.
(11) Ghobril, C.; Grinstaff, M. W. The chemistry and engineering of polymeric hydrogel adhesives for wound closure: a tutorial. *Chem. Soc. Rev.* **2015**, *44* (7), 1820−1835.
(12) El-Husseiny, H. M.; Mady, E. A.; Hamabe, L.; Abugomaa, A.; Shimada, K.; Yoshida, T.; Tanaka, T.; Yokoi, A.; Elbadawy, M.; Tanaka, R. Smart/stimuli-responsive hydrogels: Cutting-edge platforms for tissue engineering and other biomedical applications. *Mater. Today Bio* **2022**, *13*, No. 100186.
(13) Xue, X.; Hu, Y.; Wang, S. C.; Chen, X.; Jiang, Y. Y.; Su, J. C. Fabrication of physical and chemical crosslinked hydrogels for bone tissue engineering. *Bioact. Mater.* **2022**, *12*, 327−339.
(14) Zhao, Y.; Song, S.; Ren, X.; Zhang, J.; Lin, Q.; Zhao, Y. Supramolecular Adhesive Hydrogels for Tissue Engineering Applications. *Chem. Rev.* **2022**, *122* (6), 5604−5640.
(15) Liu, J.; Wu, M.; Lu, J.; He, Q.; Zhang, J. Janus Intelligent Antibacterial Hydrogel Dressings for Chronic Wound Healing in Diabetes. *ACS Appl. Polym. Mater.* **2023**, *5* (4), 2596−2606.
(16) Ribeiro, M. P.; Espiga, A.; Silva, D.; Baptista, P.; et al. Development of a New Chitosan Hydrogel for Wound Dressing. *Wound Repair Regen.* **2009**, *17*, 817−824.
(17) Alavarse, A. C.; Frachini, E. C. G.; da Silva, R. L. C. G.; Lima, V. H.; Shavandi, A.; Petri, D. F. S. Crosslinkers for polysaccharides and proteins: Synthesis conditions, mechanisms, and crosslinking efficiency, a review. *Int. J. Biol. Macromol.* **2022**, *202*, 558−596.
(18) Fatimi, A.; Okoro, O. V.; Podstawczyk, D.; Siminska-Stanny, J.; Shavandi, A. Natural Hydrogel-Based Bio-Inks for 3D Bioprinting in Tissue Engineering: A Review. *Gels* **2022**, *8* (3), No. 179.
(19) Yang, Q.; Peng, J. R.; Xiao, H. T.; Xu, X. W.; Qian, Z. Y. Polysaccharide hydrogels: Functionalization, construction and served as scaffold for tissue engineering. *Carbohydr. Polym.* **2022**, *278*, No. 118952, DOI: 10.1016/j.carbpol.2021.118952.
(20) Li, Y.; Peng, W.; Dong, Y.; Fan, B.; Qian, W.; Ji, X.; Lu, X.; Gan, D.; Liu, P. Mussel-Inspired PEDOT-Incorporated Gelatin-Based Conductive Hydrogel with Flexibility and Electroactivity to Accelerate Wound Healing In Vitro. *ACS Appl. Polym. Mater.* **2023**, *5* (6), 4233−4243.
(21) Gómez-Guillén, M.; Giménez, B.; López-Caballero, M. E.; Montero, M. P. Functional and bioactive properties of collagen and

gelatin from alternative sources: A review. *Food Hydrocolloids* **2011**, *25* (8), 1813−1827.
(22) Liang, Y.; He, J.; Guo, B. Functional Hydrogels as Wound Dressing to Enhance Wound Healing. *ACS Nano* **2021**, *15* (8), 12687−12722.
(23) Zhang, X.; Do, M. D.; Casey, P.; Sulistio, A.; Qiao, G. G.; Lundin, L.; Lillford, P.; Kosaraju, S. Chemical Cross-Linking Gelatin with Natural Phenolic Compounds as Studied by High-Resolution NMR Spectroscopy. *Biomacromolecules* **2010**, *11* (4), 1125−1132.
(24) Ilkar Erdagi, S.; Ngwabebhoh, F. A.; Yildiz, U. Genipin crosslinked gelatin-diosgenin-nanocellulose hydrogels for potential wound dressing and healing applications. *Int. J. Biol. Macromol.* **2020**, *149*, 651−663.
(25) Jayakrishnan, A.; Jameela, S. R. Glutaraldehyde as a fixative in bioprostheses and drug delivery matrices. *Biomaterials* **1996**, *17* (5), 471−484.
(26) Draye, J. P.; Delaey, B.; Van de Voorde, A.; Van Den Bulcke, A.; De Reu, B.; Schacht, E. In vitro and in vivo biocompatibility of dextran dialdehyde cross-linked gelatin hydrogel films. *Biomaterials* **1998**, *19* (18), 1677−1687.
(27) Van Den Bulcke, A. I.; Bogdanov, B.; De Rooze, N.; Schacht, E. H.; Cornelissen, M.; Berghmans, H. Structural and Rheological Properties of Methacrylamide Modified Gelatin Hydrogels. *Biomacromolecules* **2000**, *1* (1), 31−38.
(28) Sani, E. S.; Kheirkhah, A.; Rana, D.; Sun, Z.; Foulsham, W.; Sheikhi, A.; Khademhosseini, A.; Dana, R.; Annabi, N. Sutureless repair of corneal injuries using naturally derived bioadhesive hydrogels. *Sci. Adv.* **2019**, *5* (3), No. eaav1281.
(29) Jaiswal, M. K.; Xavier, J. R.; Carrow, J. K.; Desai, P.; Alge, D.; Gaharwar, A. K. Mechanically Stiff Nanocomposite Hydrogels at Ultralow Nanoparticle Content. *ACS Nano* **2016**, *10* (1), 246−256.
(30) Assmann, A.; Vegh, A.; Ghasemi-Rad, M.; Bagherifard, S.; Cheng, G.; Sani, E. S.; Ruiz-Esparza, G. U.; Noshadi, I.; Lassaletta, A. D.; Gangadharan, S.; et al. A highly adhesive and naturally derived sealant. *Biomaterials* **2017**, *140*, 115−127.
(31) Eke, G.; Mangir, N.; Hasirci, N.; MacNeil, S.; Hasirci, V. Development of a UV crosslinked biodegradable hydrogel containing adipose derived stem cells to promote vascularization for skin wounds and tissue engineering. *Biomaterials* **2017**, *129*, 188−198.
(32) Jalili, N. A.; Jaiswal, M. K.; Peak, C. W.; Cross, L. M.; Gaharwar, A. K. Injectable nanoengineered stimuli-responsive hydrogels for on-demand and localized therapeutic delivery. *Nanoscale* **2017**, *9* (40), 15379−15389.
(33) Adib, A. A.; Sheikhi, A.; Shahhosseini, M.; Simeunović, A.; Wu, S.; Castro, C. E.; Zhao, R.; Khademhosseini, A.; Hoelzle, D. J. Direct-write 3D printing and characterization of a GelMA-based biomaterial for intracorporeal tissue engineering. *Biofabrication* **2020**, *12* (4), No. 045006.
(34) Liu, H.; Zhu, X.; Guo, H.; Huang, H.; Huang, S.; Huang, S.; Xue, W.; Zhu, P.; Guo, R. Nitric oxide released injectable hydrogel combined with synergistic photothermal therapy for antibacterial and accelerated wound healing. *Appl. Mater. Today* **2020**, *20*, No. 100781.
(35) Elkhoury, K.; Morsink, M.; Tahri, Y.; Kahn, C.; Cleymand, F.; Shin, S. R.; Arab-Tehrany, E.; Sanchez-Gonzalez, L. Synthesis and characterization of C2C12-laden gelatin methacryloyl (GelMA) from marine and mammalian sources. *Int. J. Biol. Macromol.* **2021**, *183*, 918−926.
(36) Wang, K.-Y.; Jin, X.-Y.; Ma, Y.-H.; Cai, W.-J.; Xiao, W.-Y.; Li, Z.-W.; Qi, X.; Ding, J. Injectable stress relaxation gelatin-based hydrogels with positive surface charge for adsorption of aggrecan and facile cartilage tissue regeneration. *J. Nanobiotechnol.* **2021**, *19* (1), No. 214.
(37) Kurian, A. G.; Singh, R. K.; Patel, K. D.; Lee, J.-H.; Kim, H.-W. Multifunctional GelMA platforms with nanomaterials for advanced tissue therapeutics. *Bioact. Mater.* **2022**, *8*, 267−295.
(38) Liu, J.; Qu, M.; Wang, C.; Xue, Y.; Huang, H.; Chen, Q.; Sun, W.; Zhou, X.; Xu, G.; Jiang, X. A Dual-Cross-Linked Hydrogel Patch for Promoting Diabetic Wound Healing. *Small* **2022**, *18* (17), No. 2106172.
(39) Martineau, L.; Peng, H.; Shek, P. *Development of a Novel Biomaterial: Part II. Evaluation of a Photo Cross-linking Method*; Defence Research & Development Canada: Toronto, 2023.
(40) Hong, Y.; Zhou, F.; Hua, Y.; Zhang, X.; Ni, C.; Pan, D.; Zhang, Y.; Jiang, D.; Yang, L.; Lin, Q.; et al. A strongly adhesive hemostatic hydrogel for the repair of arterial and heart bleeds. *Nat. Commun.* **2019**, *10* (1), No. 2060.
(41) Davoodi, P.; Lee, L. Y.; Xu, Q.; Sunil, V.; Sun, Y.; Soh, S.; Wang, C.-H. Drug delivery systems for programmed and on-demand release. *Adv. Drug Delivery Rev.* **2018**, *132*, 104−138.
(42) Merino, S.; Martín, C.; Kostarelos, K.; Prato, M.; Vázquez, E. Nanocomposite Hydrogels: 3D Polymer−Nanoparticle Synergies for On-Demand Drug Delivery. *ACS Nano* **2015**, *9* (5), 4686−4697.
(43) Li, J.; Mooney, D. J. Designing hydrogels for controlled drug delivery. *Nat. Rev. Mater.* **2016**, *1* (12), No. 16071.
(44) Li, Z.; Ye, E.; David; Lakshminarayanan, R.; Loh, X. J. Recent Advances of Using Hybrid Nanocarriers in Remotely Controlled Therapeutic Delivery. *Small* **2016**, *12* (35), 4782−4806.
(45) Narayanaswamy, R.; Torchilin, V. P. Hydrogels and Their Applications in Targeted Drug Delivery. *Molecules* **2019**, *24* (3), No. 603, DOI: 10.3390/molecules24030603.
(46) Dreiss, C. A. Hydrogel design strategies for drug delivery. *Curr. Opin. Colloid Interface Sci.* **2020**, *48*, 1−17.
(47) Sonker, M.; Bajpai, S.; Khan, M. A.; Yu, X.; Tiwary, S. K.; Shreyash, N. Review of Recent Advances and Their Improvement in the Effectiveness of Hydrogel-Based Targeted Drug Delivery: A Hope for Treating Cancer. *Acs Appl. Bio Mater.* **2021**, *4* (12), 8080−8109.
(48) Li, J. Self-assembled supramolecular hydrogels based on polymer−cyclodextrin inclusion complexes for drug delivery. *NPG Asia Mater.* **2010**, *2* (3), 112−118.
(49) Liu, J.; Tian, B.; Liu, Y.; Wan, J.-B. Cyclodextrin-Containing Hydrogels: A Review of Preparation Method, Drug Delivery, and Degradation Behavior. *Int. J. Mol. Sci.* **2021**, *22* (24), No. 13516, DOI: 10.3390/ijms222413516.
(50) Omtvedt, L. A.; Kristiansen, K. A.; Strand, W. I.; Aachmann, F. L.; Strand, B. L.; Zaytseva-Zotova, D. S. Alginate hydrogels functionalized with β-cyclodextrin as a local paclitaxel delivery system. *J. Biomed. Mater. Res., Part A* **2021**, *109* (12), 2625−2639.
(51) Yang, Q.; Gao, C.; Zhang, X.; Tsou, C.; Zhao, X.; De Guzman, M. R.; Pu, Z.; Li, X.; Lu, Y.; Zeng, C.; et al. A Dual Physical Cross-Linking Strategy to Construct Tough Hydrogels with High Strength, Excellent Fatigue Resistance, and Stretching-Induced Strengthening Effect. *Macromol. Mater. Eng.* **2021**, *306* (7), No. 2100093, DOI: 10.1002/mame.202100093.
(52) Ren, P.; Wei, D.; Liang, M.; Xu, L.; Zhang, T.; Zhang, Q. Alginate/gelatin-based hybrid hydrogels with function of injecting and encapsulating cells in situ. *Int. J. Biol. Macromol.* **2022**, *212*, 67−84.
(53) Moncada-Basualto, M.; Matsuhiro, B.; Mansilla, A.; Lapier, M.; Maya, J. D.; Olea-Azar, C. Supramolecular hydrogels of β-cyclodextrin linked to calcium homopoly-L-guluronate for release of coumarins with trypanocidal activity. *Carbohydr. Polym.* **2019**, *204*, 170−181.
(54) Thi, T. T. H.; Lee, Y.; Ryu, S. B.; Sung, H.-J.; Park, K. D. Oxidized cyclodextrin-functionalized injectable gelatin hydrogels as a new platform for tissue-adhesive hydrophobic drug delivery. *RSC Adv.* **2017**, *7* (54), 34053−34062.
(55) Jensen, B. E. B.; Dávila, I.; Zelikin, A. N. Poly(vinyl alcohol) Physical Hydrogels: Matrix-Mediated Drug Delivery Using Spontaneously Eroding Substrate. *J. Phys. Chem. B* **2016**, *120* (26), 5916−5926.
(56) Dai, X.; Zhang, Y.; Gao, L.; Bai, T.; Wang, W.; Cui, Y.; Liu, W. A Mechanically Strong, Highly Stable, Thermoplastic, and Self-Healable Supramolecular Polymer Hydrogel. *Adv. Mater.* **2015**, *27* (23), 3566−3571.
(57) Huang, Y.; Zhai, X.; Ma, T.; Zhang, M.; Yang, H.; Zhang, S.; Wang, J.; Liu, W.; Jin, X.; Lu, W. W.; et al. A Unified Therapeutic−Prophylactic Tissue-Engineering Scaffold Demonstrated to Prevent Tumor Recurrence and Overcoming Infection toward Bone Remodeling. *Adv. Mater.* **2023**, *35* (25), No. 2300313.

(58) Fan, C.; Liu, B.; Xu, Z.; Cui, C.; Wu, T.; Yang, Y.; Zhang, D.; Xiao, M.; Zhang, Z.; Liu, W. Polymerization of N-acryloylsemicarbazide: a facile and versatile strategy to tailor-make highly stiff and tough hydrogels. *Mater. Horiz.* **2020**, *7* (4), 1160−1170.
(59) Li, J.; Ma, Q.; Xu, Y.; Yang, M.; Wu, Q.; Wang, F.; Sun, P. Highly Bidirectional Bendable Actuator Engineered by LCST−UCST Bilayer Hydrogel with Enhanced Interface. *ACS Appl. Mater. Interfaces* **2020**, *12*, 55290−55298.
(60) Liu, T.; Bao, B.; Li, Y.; Lin, Q.; Zhu, L. Photo-responsive Polymers based on *o*-Nitrobenzyl Derivatives: From Structural Design to Applications. *Prog. Polym. Sci.* **2023**, *146*, No. 101741.
(61) Zhang, J.; Si, D.; Wang, S.; Chen, X.; Zhou, H.; Yang, M. Photo-induced hydrogen-bonding complexes for drug periodic release. *Biomater. Sci.* **2019**, *7* (6), 2468−2479.
(62) Zhang, J.; Wang, S.; Zhao, Z.; Si, D.; Zhou, H.; Yang, M.; Wang, X. An In situ Forming Hydrogel Based on Photo-Induced Hydrogen Bonding. *Macromol. Res.* **2020**, *28* (12), 1127−1133.
(63) Habeeb, A. F. S. A. Determination of free amino groups in proteins by trinitrobenzenesulfonic acid. *Anal. Biochem.* **1966**, *14* (3), 328−336.
(64) Shim, J. H.; Cheun, S. H.; Kim, H. S.; Ha, D.-C. Organocatalysis for the Asymmetric Michael Addition of Aldehydes and *α*,*β*-Unsaturated Nitroalkenes. *Catalysts* **2022**, *12* (2), No. 121.
(65) Lin, C.-H.; Su, J. J.-M.; Lee, S.-Y.; Lin, Y.-M. Stiffness modification of photopolymerizable gelatin-methacrylate hydrogels influences endothelial differentiation of human mesenchymal stem cells. *J. Tissue Eng. Regener. Med.* **2018**, *12* (10), 2099−2111.
(66) Annabi, N.; Nichol, J. W.; Zhong, X.; Ji, C.; Koshy, S.; Khademhosseini, A.; Dehghani, F. Controlling the Porosity and Microarchitecture of Hydrogels for Tissue Engineering. *Tissue Eng., Part B* **2010**, *16* (4), 371−383.
(67) Peppas, N. A.; Hilt, J. Z.; Khademhosseini, A.; Langer, R. Hydrogels in Biology and Medicine: From Molecular Principles to Bionanotechnology. *Adv. Mater.* **2006**, *18* (11), 1345−1360.
(68) Gowda, A. H. J.; Bu, Y.; Kudina, O.; Krishna, K. V.; Bohara, R. A.; Eglin, D.; Pandit, A. Design of tunable gelatin-dopamine based bioadhesives. *Int. J. Biol. Macromol.* **2020**, *164*, 1384−1391.
(69) Anjani, Q. K.; Permana, A. D.; Cárcamo-Martínez, A.; Domínguez-Robles, J.; Tekko, I. A.; Larrañeta, E.; Vora, L. K.; Ramadon, D.; Donnelly, R. F. Versatility of hydrogel-forming microneedles in in vitro transdermal delivery of tuberculosis drugs. *Eur. J. Pharm. Biopharm.* **2021**, *158*, 294−312.
(70) Bharathi, R.; Ganesh, S. S.; Harini, G.; Vatsala, K.; Anushikaa, R.; Aravind, S.; Abinaya, S.; Selvamurugan, N. Chitosan-based scaffolds as drug delivery systems in bone tissue engineering. *Int. J. Biol. Macromol.* **2022**, *222*, 132−153.

https://doi.org/10.1021/acsomega.4c01963
ACS Omega 2024, 9, 34413−34427